JPhys Materials

PAPER • OPEN ACCESS

Extreme in-plane thermal conductivity anisotropy in Rhenium-based dichalcogenides

To cite this article: Sina Tahbaz and Simone Pisana 2024 *J. Phys. Mater.* **7** 015014

Journal of Physics: Materials

PAPER

Extreme in-plane thermal conductivity anisotropy in Rhenium-based dichalcogenides

Sina Tahbaz and Simone Pisana*

Department of Electrical Engineering and Computer Science, York University, 4700 Keele St, Toronto, ON M3J 1P3, Canada
* Author to whom any correspondence should be addressed.

E-mail: pisana@yorku.ca

Keywords: frequency domain thermoreflectance, transition metal dichalcogenide, thermal conductivity, rhenium disulfide, rhenium diselenide

Supplementary material for this article is available online

OPEN ACCESS

RECEIVED
9 September 2023

REVISED
24 December 2023

ACCEPTED FOR PUBLICATION
11 January 2024

PUBLISHED
19 January 2024

Abstract

Anisotropies in thermal conductivity are important for thermal management in a variety of applications, but also provide insight on the physics of nanoscale heat transfer. As materials are discovered with more extreme transport properties, it is interesting to ask what the limits are for how dissimilar the thermal conductivity can be along different directions in a crystal. Here we report on the thermal properties of rhenium-based transition metal dichalcogenides (TMDs), specifically rhenium disulfide (ReS_2) and rhenium diselenide ($ReSe_2$), highlighting their extraordinary thermal conductivity anisotropy. Along the basal crystal plane of ReS_2, a maximum of $169 \pm 11\ W\ mK^{-1}$ is detected along the *b*-axis and a minimum of $53 \pm 4\ W\ mK^{-1}$ perpendicular to it. For $ReSe_2$, the maximum and minimum values of $116 \pm 3\ W\ mK^{-1}$ and $27 \pm 1\ W\ mK^{-1}$ are found to lie 60° and 150° away from the *b*-axis, along the polarization direction of some of the principal Raman modes. These measurements demonstrate a remarkable anisotropy of 3.2 × and 4.3 × in the conductivity *within* the crystal basal planes, respectively. The through-plane thermal conductivities, recorded at $0.66 \pm 0.01\ W\ mK^{-1}$ for ReS_2 and $2.31 \pm 0.01\ W\ mK^{-1}$ for $ReSe_2$, highlight the impact of their layered structures, contributing to notably high in-plane to through-plane thermal conductivity ratios of 256 × for ReS_2 and 50 × for $ReSe_2$. This research demonstrates the unique thermal properties that these comparatively underexplored TMDs have, shedding light on the need for further exploration into the intricate thermal behavior of such materials, while underscoring their potential significance for future applications in the fields of semiconductor devices and nanotechnology.

1. Introduction

Transition metal dichalcogenides (TMDs) are a diverse and promising group of two-dimensional (2D) materials that manifest semiconducting properties [1]. Composed of a transition metal (e.g. molybdenum (Mo), tungsten (W), or rhenium (Rh)) and a chalcogen atom (sulfur (S), selenium (Se), or tellurium (Te)), TMDs have invoked considerable scientific interest owing to their unique and often tunable electronic and optical properties, with applications envisioned in optoelectronic and energy harvesting devices [2]. Extensive research has been conducted on the thermal properties of TMDs [3–8] such as MoS_2 and WS_2. Common features of the thermal conductivity of TMDs include high anisotropy with larger thermal conductivity along the basal plane of the layered crystal, due to the weaker bonds found across the plane, lower conductivities for TMDs composed of heavier chalcogen atoms, and long phonon mean free paths at room temperature. Rhenium-based TMDs, specifically ReS_2 and $ReSe_2$, have received considerably less attention. While the thermal conductivity of ReS_2 has been investigated by Jang *et al* [9], $ReSe_2$ remains largely unexplored experimentally. A defining characteristic of ReS_2 and $ReSe_2$ is their crystal structure, being triclinic with a more complex unit cell and hence less symmetric than the more common hexagonal TMD crystal configurations. The lack of crystal symmetry naturally leads to more complex anisotropies. Indeed,

Jang *et al* [9]. measured ReS_2 to have a thermal conductivity along the Re atomic chains (along the *b*-axis) to be 1.4 × larger than the orthogonal in-plane direction, and 130 × larger than the through-plane direction.

Theoretical studies of the thermal properties of both of these materials have been very limited thus far. Tongay *et al* [10]. performed density functional theory calculations of the structure and phonon dispersion of ReS_2, showing how the layers constituting the bulk crystal are unusually decoupled, leading to estimated values of thermal conductivity 70 W mK^{-1} in-plane and very low conductivity of 0.05 W mK^{-1} through the plane. In the case of $ReSe_2$, a study by Mahmoud and Joubert [11]. reports a thermal conductivity of approximately 18 W mK^{-1} in the *a*-axis and 0.69 W mK^{-1} along the *c*-axis. Bang *et al* [12] instead reports theoretical values of about 9 W mK^{-1} in-plane and 2 W mK^{-1} through-plane. None of these theoretical studies report any appreciable in-plane anisotropy, in contrast to the experimental results of Jang *et al* [9].

This work aims to further elucidate on the thermal conductivity of these TMDs. As it will be shown later, a significant observation from this study is the distinctively high in-plane anisotropy manifested by both ReS_2 and $ReSe_2$, which is a record in comparison to other TMDs and 2D materials in general.

2. Anisotropic thermal conductivity measurement

Frequency domain thermoreflectance (FDTR) is an experimental technique extensively used to measure thermal properties, especially thermal conductivity, of various materials [13–17]. This non-destructive, optically-based method primarily involves inducing and monitoring temperature oscillations within the material under study, providing insights into its thermal response [18]. In FDTR a pump laser beam is modulated at a certain frequency and focused on the surface of a sample, inducing periodic thermal waves that propagate through the material. The probe beam, reflected off the sample's surface, detects the resulting surface temperature oscillations via changes in its reflectance—an effect known as thermoreflectance. By analyzing the phase lag and amplitude of the thermoreflectance signal as a function of the modulation frequency, the thermal conductivity of the material can be inferred. In the majority of FDTR implementations, a thin metallic transducer made of aluminum or gold is deposited on the surface of the sample, thus providing an opaque layer that efficiently absorbs the pump energy near the surface of the sample, and providing transduction through a high thermoreflectance coefficient such that changes in the surface temperature can be detected as reflectance variations. Our FDTR implementation has been described in detail elsewhere [19]. Briefly, our setup operates on a 515 nm pump and a 785 nm probe laser. The laser beams are focused onto the sample using a 10 × objective, resulting in a spot size of 5.8 μm for the pump and 2.5 μm for the probe beam measured using razor profiling. The pump beam is modulated from a few kHz up to tens of MHz to span frequencies with the highest sensitivity to the thermal conductivity of the samples. Two different measurements are made in order to recover the thermal phase response of the sample. A first measurement made by detecting the probe beam gathers data from the sample, and a subsequent reference measurement made by detecting the pump beam after reflection from the sample allows us to subtract the phase shifts in the probe signal that are due to the optical path of the laser beams and the electronics [19]. The thermal phase response of the sample obtained by subtracting these two measurements is then fitted to a model to obtain the desired thermal properties of the sample.

While conventional FDTR provides valuable data on the thermal properties of the material and can distinguish in-plane from through-plane transport, it does not differentiate the thermal characteristics along different in-plane directions. To overcome this limitation, beam-offset FDTR (BO-FDTR)[19–21] is employed. In BO-FDTR, a spatial offset is introduced between the pump and the probe beam, making the measurement more sensitive to the thermal conductivity in the direction of the offset. This configuration allows sampling the thermal waves that propagate laterally across the material, effectively enabling the extraction of direction-dependent thermal properties. The BO-FDTR technique thus offers a more nuanced investigation of in-plane anisotropy, making it particularly suitable for studying materials like ReS_2 and $ReSe_2$ where this anisotropy is quite large. In order to create the offset between the two beams in our setup, the pump beam passes through a 12 mm thick glass window mounted on a linear actuator that rotates the glass window. Light propagating through the glass window will therefore be refracted and offset laterally in proportion to the window thickness and angle of incidence, without affecting the direction of propagation. The resulting beam offset is 3.7 μm on the sample surface for a 6 mm actuator displacement, as determined by razor profiling the focused beam at the focal location as function of actuator displacement. A diagram of the experimental setup is provided in the supplementary information.

2.1. Modeling FDTR data

The method used to extract the thermophysical parameters of interest from FDTR is well documented in the literature [18, 22]. It involves using the frequency-domain solution of Fourier's Law in cylindrical

coordinated in layered media, and weighting the response according to the pump and probe beams' Gaussian shape. Generally, the sample's thermal response is modeled by specifying thermal conductivity (κ), thickness (h) and volumetric heat capacity (C_v) for each layer, and thermal boundary conductance (G) of each interface. All parameters are assumed to be known except for the unknowns of interest. In the present study, we implemented the solution that takes into account for beam offsets in anisotropic media initially developed by Feser *et al* [23], which generalized κ to be a 3×3 tensor. The tensorial representation, together with beam-offsetting, allows us to resolve κ in distinct directions both within the plane of the sample (in-plane) and perpendicular to it (through-plane). We note that a 3×3 κ-tensor for a triclinic crystal has no zero elements, and due to Onsager's Theorem the tensor is symmetric, leading to a tensor of the form

$$\begin{bmatrix} \kappa_{xx} & \kappa_{xy} & \kappa_{xz} \\ \kappa_{xy} & \kappa_{yy} & \kappa_{yz} \\ \kappa_{xz} & \kappa_{yz} & \kappa_{zz} \end{bmatrix} \tag{1}$$

where the indices are defined according to $q_i = -\kappa_{ij}\frac{\partial T}{\partial j}$, q is the heat flux along i giving rise to a temperature (T) gradient along j. Equation (1) specifies three spatially orthogonal values for κ and three angles with respect to the coordinate system of the FDTR experiment. We cannot simultaneously solve for all these unknowns in our experiment. However, we make the approximation that the c-axis is perpendicular to the plane of the substrate on which the crystal is placed and that the a and b axes are nearly orthogonal to the c-axis. These approximations are supported by the fact that layered crystals like TMDs cleave more easily across the c-axis and the unit cell angles with respect to the c-axis are 88° and 75° for ReS_2 and 92° and 104° for $ReSe_2$. This implies that within our approximation we can take the orientation of the crystal to have the c-axis perpendicular to the substrate, and approximate $\kappa_{xz} \approx \kappa_{yz} \approx 0$. Proceeding this way, the remaining unknowns are κ_{xx}, κ_{yy}, κ_{zz} and the angle of the basal plane of the crystal with respect to the FDTR offset direction that gives rise to κ_{xy}. The basal plane orientation is uniquely identified by polarized Raman spectroscopy. For simplicity, in the remained of the paper we will refer to κ_z as the through-plane thermal conductivity and take that to be along the c-axis, and $\kappa_r(\theta)$ represents the angle-dependent thermal conductivity along the basal plane of the crystal.

We take measurements of the thermal phase of the sample as function of modulation frequency for a fixed pump-probe offset, and change the offset direction with respect to a sample's crystal orientation by rotating the sample. For each offset direction, we fit for κ_x (the in-plane conductivity in the direction of the beam offset), κ_y (the in-plane conductivity in the direction perpendicular to the beam offset) and κ_z (the through-plane conductivity). Then $\kappa_r(\theta) = [\kappa_x(\theta) + \kappa_y(\theta + 90°)]/2$. This allows us to take the average of equivalent results of the fits. All other thermophysical parameters are taken as known. Namely, the transducer thin film properties are determined on areas of the substrate without the crystal, together with the substrate properties, as explained below. The full list of parameters used in the model, sample FDTR data with corresponding model fits, reference measurements to obtain parameters that were held constant are given in the supplementary information, together with sensitivity analysis of our measurement to the parameters of interest and fitted parameter dependency.

2.2. Sample preparation and characterization

Samples of $ReSe_2$ and ReS_2, were prepared via slightly different methodologies, although either approach yields equivalent results. Bulk crystals were procured from 2D semiconductors.

The preparation of the $ReSe_2$ flakes was done by mechanical exfoliation [24], a popular technique employed in the preparation of 2D materials [25, 26]. After exfoliation, the flake was transferred to Kapton tape, which was firmly secured with double-sided tape on a glass slide. Subsequently, this assembly was coated with a layer of ~50 nm Al via electron-beam deposition.

The ReS_2 crystal was also mechanically exfoliated. However, instead of transferring the exfoliated flakes to a Kapton tape support, they were transferred to a 300 nm SiO_2 / Si substrate. The transfer of flakes onto this substrate was accomplished through the use of thermal release tape [27, 28] at a temperature of 105 ° C. This method was utilized to obtain larger flake sizes. Following the transfer, the flakes were coated with a ~50 nm layer of Al by sputter deposition.

The thickness of the flakes were determined using a Bruker optical profilometer. The flakes had a thickness of ~3 μm for the ReS_2 and ~10 μm for $ReSe_2$ as evident in figures 1(b) and 2(b), respectively. The flakes are thus thick enough that entirely diffusive transport is expected at room temperature, since a thickness dependence of κ would arise when the thickness is of the order of the phonon mean free paths. No dependence was detected in ReS_2, for example, down to a thickness of 60 nm [9]. Furthermore, the diffusive thermal wave penetration in the through-plane direction is given by $\sqrt{\kappa_z/\pi C_v f}$ and estimated to be within

~1.7 μm for ReS_2 and ~8 μm for $ReSe_2$. Therefore, even for the lowest modulation frequencies used in our FDTR measurements (35 kHz for ReS_2 and 5 kHz for $ReSe_2$), the presence of the bottom crystal boundary would not be detected. This is supported by the fact that the FDTR model fits are independent of the presence of the substrate in the model, thus the crystals can be taken as being semi-infinite.

Polarized Raman spectra [29] were collected with a Renishaw inVia Reflex at 532 nm for each of the flakes prior to deposition of the Al layer. The flakes were rotated in 15° steps relative to the polarization of the Raman beam [30] and the intensity of the prominent peaks for each material were recorded, allowing for the identification of the crystal axes.

3. Results and discussion

Figures 1(e) and (f) reveal a clear angular dependence in the intensity of the Raman peaks with respect to the direction of the crystal, as previously reported [29, 31]. The flakes have been aligned such that the 0° angle in plots correlates with the horizontal edge of the flakes as seen in figure 1(a). The longer horizontal edges have been shown to be likely directions on the *b*-axis of the crystal, due to preferential cleaving along that direction [32]. This general observation is verified by analysis of the Raman peaks, as the peaks of specific Raman modes have highest intensity when the Raman polarization direction is aligned with one of the principal axes of the crystal. For example, mode *V* at 209 cm^{-1} has been shown to be most intense when the laser polarization is aligned with the *b*-axis of the ReS_2 crystal [29, 31, 33, 34]. The relative angular orientation of mode *III* at 149 cm^{-1} with respect to mode *V* indicates that the *c*-axis of the crystal is pointing down towards the substrate (the two faces of the crystal are not equivalent because of the low crystal symmetry)[29]. Based on these observations, we assign the *b*-axis to 0° (horizontal direction) in figure 1.

Our measurements reveal a notable anisotropy in the in-plane thermal conductivity $\kappa_r(\theta)$ of the examined flakes, with highest values obtained along the *b*-axis (along the Re atomic chain direction), as previously observed by Jang [9]. The value recorded for $\kappa_r(\theta = 0°) = 169 \pm 11$ W mK^{-1} is substantially higher than the values recorded by Jang of 70 ± 18 W mK^{-1}, but the value for $\kappa_r(\theta = 90°) = 53 \pm 4$ W mK^{-1} is the same within error (50 ± 13 W mK^{-1} in [9]). The high conductivity value is also found in other ReS_2 flakes we tested, and can potentially be ascribed to procuring the crystals from different sources, which can lead to differences in crystal grain size [35–37]. Indeed, in spite of large lateral grain sizes spanning hundreds of μm along the basal plane, the continuity of the crystal in the through-plane direction can be interrupted by grain boundaries or stacking faults. Such sources of boundary scattering can, similarly to limitations in the thickness of the crystal itself, play an important role in limiting κ_r and κ_z[37, 38]. Although Jang did not find variations in κ for sample thickness ranging from 60 to 450 nm, the difference with our result may be ascribed to the presence of defects on a length scale of a few tens of nm.

The measured variation in $\kappa_r(\theta)$ reveals an extremely large in-plane thermal conductivity anisotropy ratio of 3.2. In the context of TMDs [39] and 2D materials [40, 41], it is not unprecedented to observe such high values of κ_r and large anisotropies between κ_r and κ_z. However, large variations in $\kappa_r(\theta)$, that is *within* the basal plane, are less common. Black phosphorous was found to have an in-plane anisotropy of 2 [42], and so did TiS_3[43]. However, we are not aware of experimental observations with in-plane anisotropies as large as the ones reported here. The thermal conductivities of MXenes [44–46] have been predicted to have larger in-plane anisotropies. In the paper by Luo *et al* [44], the thermal conductivity of $Sc_3(CN)F_2$ is calculated to have values of 283 and 111 W mK^{-1} along different in-plane directions, leading to an in-plane anisotropy ratio of 2.55. We are not aware of such values of in-plane anisotropy being experimentally verified. Therefore, the in-plane anisotropy ratio of 3.2 found for ReS_2 appears to be a record.

The value for the through-plane conductivity κ_z is 0.66 W mK^{-1}, and in agreement with the previous results of Jang *et al* [9]. Such a low value is in itself remarkable and it has been attributed to the very weak interlayer bonding along the *c*-axis of ReS_2. The differences in in-plane and through-plane κ leads to a ratio of 256, which almost as high as that of graphite.

The results for $ReSe_2$ presented in figure 2 show even more intriguing features. The Raman spectra allow us to identify the crystal axis orientation, which again is presented here by having the Rhenium atomic chains along the *b*-axis being referred to $\theta = 0°$[29, 47]. Unlike ReS_2, there is no prominent Raman peak that is aligned with the *b*-axis, but rather it is located 60° and 90° from modes *IV* (124 cm^{-1}) and *V* (159 cm^{-1}, respectively. Also unlike ReS_2, the maximum value recorded for $\kappa_r(\theta)$ is 60° away from the *b*-axis, and along mode *IV* in the polarized Raman data. The correlation between maximum value of $\kappa_r(\theta)$ with a prominent Raman peak, which occurs along the *b*-axis for ReS_2 but not for $ReSe_2$, strongly suggests that the thermal transport anisotropy is linked to the different phonon band structure on these materials, which in turn is determined by their crystal structure. Although these Rhenium-based TMDs have a similar crystal structure,

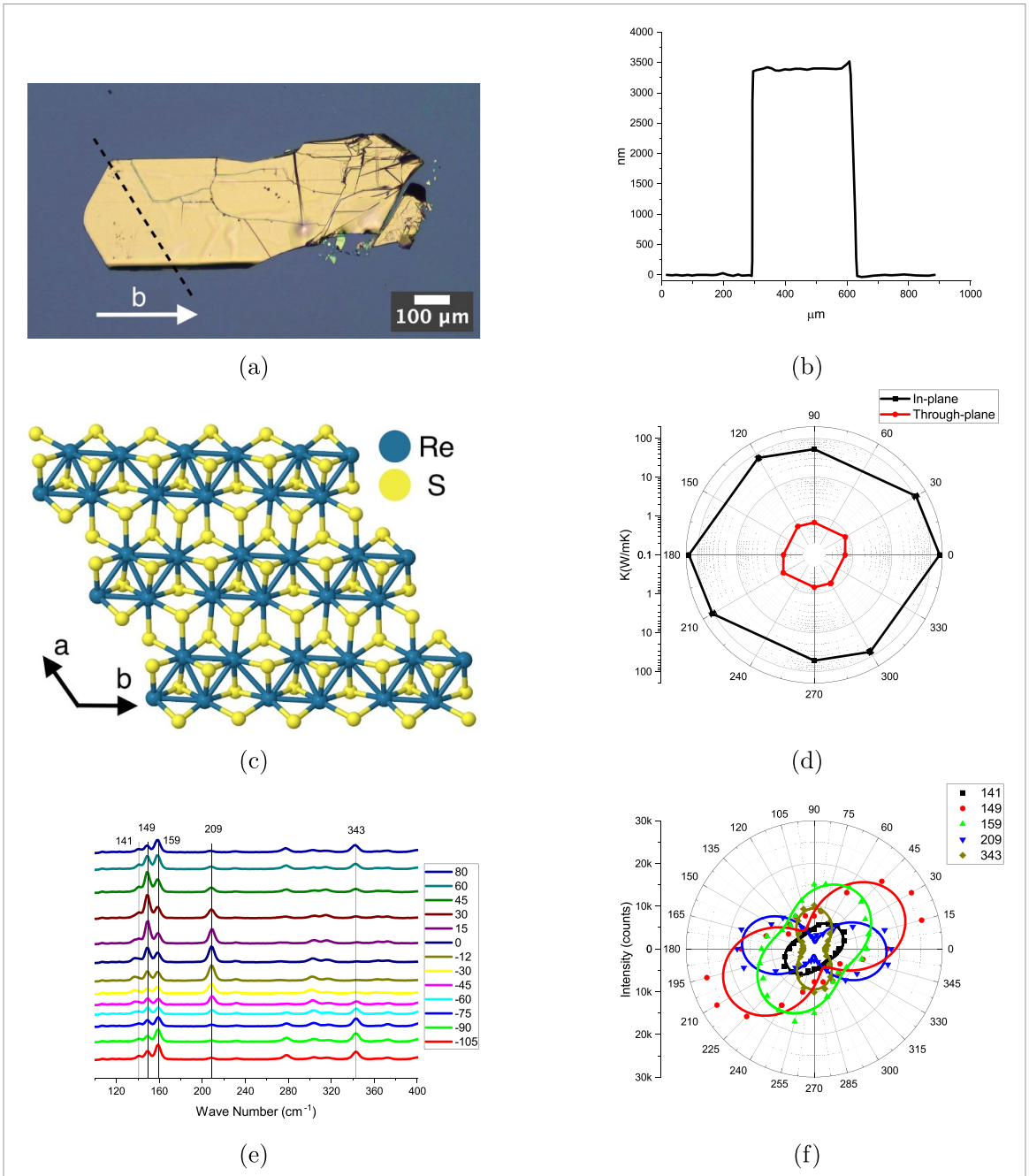

Figure 1. (a) Optical microscope image of a ReS_2 flake. (b) Optical profilometry thickness measurement of the ReS_2 flake in (a) across the line shown. (c) Crystal structure of ReS_2. (d) In-plane and through-plane thermal conductivity of ReS_2 for different angles. The 0° axis is aligned with the bottom edge of the flake in (a). (e) Polarized Raman spectroscopy of the ReS_2 flake for different rotations of the crystal with the 0° angle aligning the bottom edge of the flake in (a) to the polarization axis of the Raman laser. (f) Polar plot of the Raman intensities for the five dominant modes of ReS_2 shown in (e).

it appears that small but important variations have marked effect on the thermal transport. $ReSe_2$ exhibits generally lower value for κ_r, and this could be attributed to the larger atomic mass of selenium compared to sulfur [8], though we cannot rule out the effect of crystal quality we think is responsible for the variation in reported thermal conductivity of ReS_2. The in-plane anisotropy ratio is found to be even higher than ReS_2 at 4.3, whereas the value of κ_z is higher. We do not currently know the origin of the larger value for κ_z or the lack of monotonic variation in the recorded $\kappa_r(\theta)$ between its maximum and minimum values. It will be important to carry out theoretical modeling of the heat transport in these structures to better relate crystal and thermal properties in light of this data.

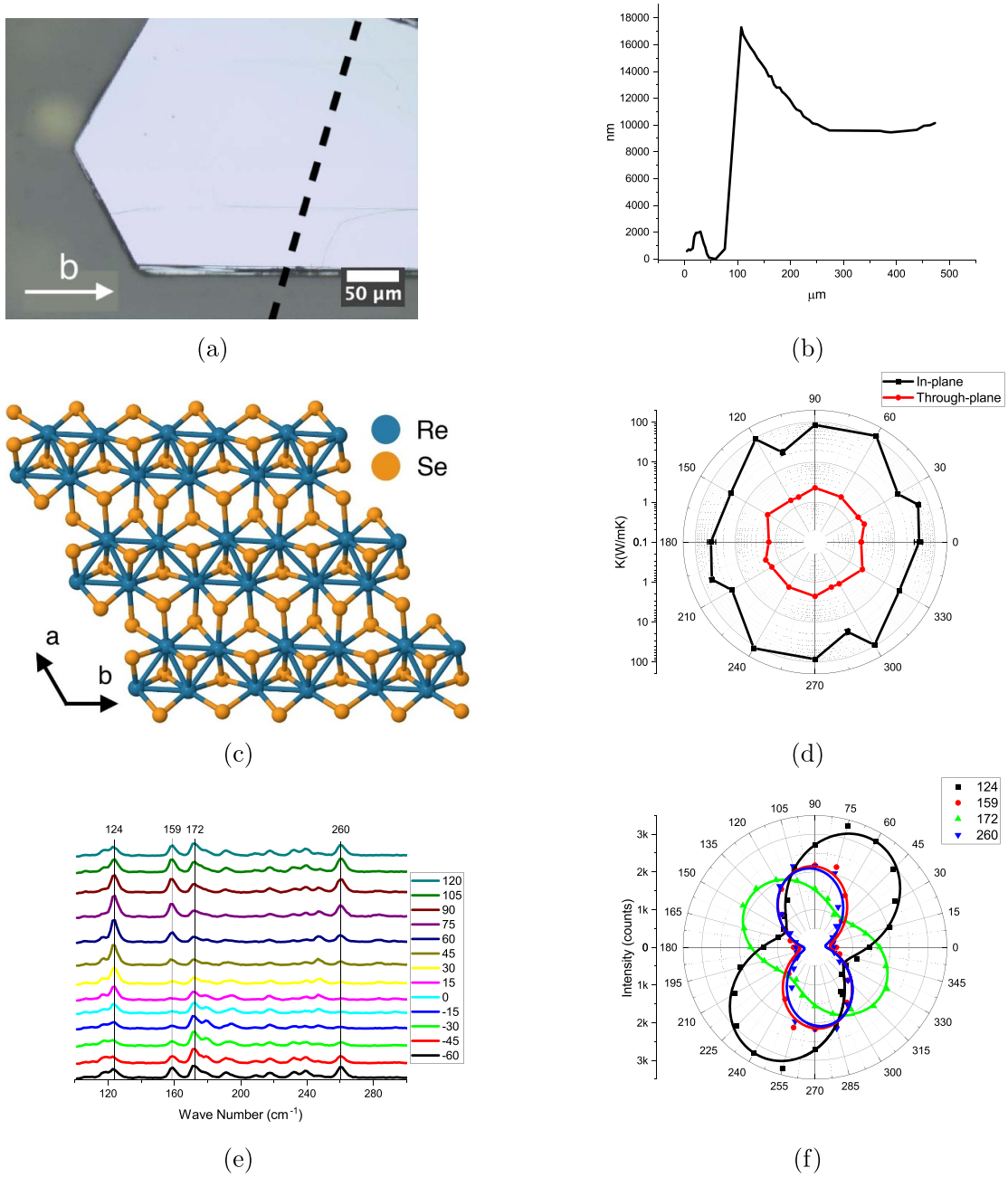

Figure 2. (a) Optical microscope image of a $ReSe_2$ flake. (b) Optical profilometry thickness measurement of the $ReSe_2$ flake in (a) across the line shown. (c) Crystal structure of $ReSe_2$. (d) In-plane and through-plane thermal conductivity of $ReSe_2$ for different angles. The 0° degree axis is aligned with the bottom edge of the flake in (a). (e) Polarized Raman spectroscopy of the $ReSe_2$ flake for different rotations of the crystal with the 0° angle aligning the bottom edge of the flake in (a) to the polarization axis of the Raman laser. (f) polar plot of the Raman intensities for the four dominant modes of $ReSe_2$ shown in (e).

4. Conclusion

In conclusion, this study provides significant insights into the thermal properties of Rhenium-based transition metal dichalcogenides (TMDs), specifically ReS_2 and $ReSe_2$, which until now remained relatively underexplored. Our results underscore an extremely high in-plane anisotropy for both ReS_2 and $ReSe_2$, a characteristic that distinguishes these materials from other TMDs and 2D materials more broadly. While ReS_2 and $ReSe_2$ share several common features such as high in-plane anisotropy, their differences have been highlighted. The findings herein open the door for further investigation into these unique materials and their potential applications in the realm of nanotechnology and semiconductor devices. Future studies should continue to explore these and other under-studied TMDs to uncover their full potential and the range of their distinct properties.

Data availability statement

The data that support the findings of this study are openly available at the following URL/DOI: https://doi.org/10.5683/SP3/UTEMIM [48].

Acknowledgments

This work has been supported by the Natural Sciences and Engineering Research Council of Canada, the Canada Foundation for Innovation and the Ontario Research Fund. We are grateful to Prof. Rodney Smith at the University of Waterloo for access to their Raman spectrometer.

ORCID iD

Simone Pisana https://orcid.org/0000-0002-9291-6061

References

[1] Manzeli S, Ovchinnikov D, Pasquier D, Yazyev O V and Kis A 2017 *Nat. Rev. Mater.* **2** 1–15
[2] Choi W, Choudhary N, Han G H, Park J, Akinwande D and Lee Y H 2017 *Mater. Today* **20** 116–30
[3] Zhang G and Zhang Y W 2017 *J. Mater. Chem.* **5** 7684–98
[4] Lu Z, Neupane G P, Jia G, Zhao H, Qi D, Du Y, Lu Y and Yin Z 2020 *Adv. Funct. Mater.* **30** 2001127
[5] Mortazavi B, Quey R, Ostadhossein A, Villani A, Moulin N, van Duin A C and Rabczuk T 2017 *Appl. Mater. Today* **7** 67–76
[6] Muratore C *et al* 2013 *Appl. Phys. Lett.* **102** 081604
[7] Ma J, Li W and Luo X 2016 *Appl. Phys. Lett.* **108** 082102
[8] Zhang Z, Xie Y, Ouyang Y and Chen Y 2017 *Int. J. Heat Mass Transfer* **108** 417–22
[9] Jang H, Ryder C R, Wood J D, Hersam M C and Cahill D G 2017 *Adv. Mater.* **29** 1700650
[10] Tongay S *et al* 2014 *Nat. Commun.* **5** 1–6
[11] Mahmoud M M and Joubert D P 2018 *Mater. Today Proc.* **5** 10424–30
[12] Bang J, Park O, Kim H S, Hwang S M, Lee S W, Park S J and Kim S I 2023 *Int. J. Energy Res.* **2023** 2831961
[13] Schmidt A J, Chen X and Chen G 2008 *Rev. Sci. Instrum.* **79** 114902
[14] Schmidt A J, Cheaito R and Chiesa M 2009 *Rev. Sci. Instrum.* **80** 094901
[15] Schmidt A J, Cheaito R and Chiesa M 2010 *J. Appl. Phys.* **107** 024908
[16] Yang J, Maragliano C and Schmidt A J 2013 *Rev. Sci. Instrum.* **84** 104904
[17] Yang J, Ziade E, Maragliano C, Crowder R, Wang X, Stefancich M, Chiesa M, Swan A K and Schmidt A J 2014 *J. Appl. Phys.* **116** 023515
[18] Cahill D G 2004 *Rev. Sci. Instrum.* **75** 5119–22
[19] Rahman M, Shahzadeh M, Braeuninger-Weimer P, Hofmann S, Hellwig O and Pisana S 2018 *J. Appl. Phys.* **123** 245110
[20] Feser J P and Cahill D G 2012 *Rev. Sci. Instrum.* **83** 104901
[21] Tang L and Dames C 2021 *Int. J. Heat Mass Transfer* **164** 120600
[22] Liu J, Zhu J, Tian M, Gu X, Schmidt A and Yang R 2013 *Rev. Sci. Instrum.* **84** 034902
[23] Feser J P, Liu J and Cahill D G 2014 *Rev. Sci. Instrum.* **85** 104903
[24] Li Y, Kuang G, Jiao Z, Yao L and Duan R 2022 *Mater. Res. Express* **9** 122001
[25] Magda G Z, Petö J, Dobrik G, Hwang C, Biró L P and Tapasztó L 2015 *Sci. Rep.* **5** 14714
[26] Watson A J, Lu W, Guimarães M H and Stöhr M 2021 *2D Mater.* **8** 032001
[27] Li Y *et al* 2022 *Nanoscale* **14** 7484–92
[28] Ooi S and Ahmad H 2022 *Opt. Mater.* **128** 112363
[29] Choi Y, Kim K, Lim S Y, Kim J, Park J M, Kim J H, Lee Z and Cheong H 2020 *Nanoscale Horiz.* **5** 308–15
[30] Hafeez M, Gan L, Bhatti A S and Zhai T 2017 *Mater. Chem. Front.* **1** 1917–32
[31] Zhang S, Mao N, Zhang N, Wu J, Tong L and Zhang J 2017 *ACS Nano* **11** 10366–72
[32] Wang H, Liu E, Wang Y, Wan B, Ho C H, Miao F and Wan X 2017 *Phys. Rev.* B **96** 165418
[33] Chenet D A, Aslan B, Huang P Y, Fan C, Van Der Zande A M, Heinz T F and Hone J C 2015 *Nano Lett.* **15** 5667–72
[34] Hart L, Dale S, Hoye S, Webb J L and Wolverson D 2016 *Nano Lett.* **16** 1381–6
[35] Li Z, Liu Y, Lindsay L, Xu Y, Duan W and Pop E 2017 arXiv:1711.02772
[36] Lindroth D O and Erhart P 2016 *Phys. Rev.* B **94** 115205
[37] Rahman M, Parvez K, Fugallo G, Dun C, Read O, Alieva A, Urban J J, Lazzeri M, Casiraghi C and Pisana S 2022 *Nanomaterials* **12** 3861
[38] Xiao P, Chavez-Angel E, Chaitoglou S, Sledzinska M, Dimoulas A, Sotomayor Torres C M and El Sachat A 2021 *Nano Lett.* **21** 9172–9
[39] Kim S E *et al* 2021 *Nature* **597** 660–5
[40] Cahill D G 2012 *MRS Bull.* **37** 855–63
[41] Yang J, Liu C, Xie H and Yu W 2021 *Nanotechnology* **32** 162001
[42] Luo Z, Maassen J, Deng Y, Du Y, Garrelts R P, Lundstrom M S, Ye P D and Xu X 2015 *Nat. Commun.* **6** 8572
[43] Liu H, Yu X, Wu K, Gao Y, Tongay S, Javey A, Chen L, Hong J and Wu J 2020 *Nano Lett.* **20** 5221–7
[44] Luo K, Zha X H, Zhou Y, Guo Z, Lin C T, Huang Q, Zhou S, Zhang R and Du S 2018 *RSC Adv.* **8** 22452–9
[45] Zha X H, Zhou J, Zhou Y, Huang Q, He J, Francisco J S, Luo K and Du S 2016 *Nanoscale* **8** 6110–7
[46] Zha X H, Huang Q, He J, He H, Zhai J, Francisco J S and Du S 2016 *Sci. Rep.* **6** 27971
[47] Wolverson D, Crampin S, Kazemi A S, Ilie A and Bending S J 2014 *ACS Nano* **8** 11154–64
[48] Pisana S and Tahbaz S 2023 Beam-offset frequency-domain thermoreflectance data of bulk Rhenium Disulfide and Rhenium Diselenide crystals Borealis (https://doi.org/10.5683/SP3/UTEMIM)